Inorganic Chemistry

pubs.acs.org/IC Article

An Inconspicuous Six-Coordinate Neutral Dy^{III} Single-Ion Magnet with Remarkable Magnetic Anisotropy and Stability

Min Li,[‖] Haipeng Wu,[‖] Zhengqiang Xia,* Liviu Ungur,* Dan Liu,* Liviu F. Chibotaru, Hongshan Ke, Sanping Chen,* and Shengli Gao

Cite This: *Inorg. Chem.* 2020, 59, 7158–7166 Read Online

ACCESS | Metrics & More | Article Recommendations | Supporting Information

ABSTRACT: It is a crucial challenge to address both magnetic anisotropy and stability for single-molecule magnets (SMMs) used in next-generation nanodevices. Highly axial lanthanide SMMs with neutral charge and moderate coordination numbers represent promising magnetic materials. Here, using iodide ions with large volume and low surface charge density as weak donors, we report a six-coordinate neutral dysprosium SMM $[Dy(Cy_3PO)_2I_3(CH_3CN)]$ with a certain degree of stability exhibiting a huge thermal barrier of 1062 K and hysteresis loops open up to 9 K. Through the elaborate reduction of ligand field strength, an apparent strongly axial crystal field is provided which elicits prominent crystal-field splitting and high axiality with the thermally activated relaxation via the third-excited Kramers' doublet. Moreover, the profound influence of strong equatorial ligand substitution on the electronic structure and relaxation pathway is clearly explored in Dy^{III} analogues. The result suggests the great potential of the reducing the transverse ligand field in the improvement of SMMs performance.

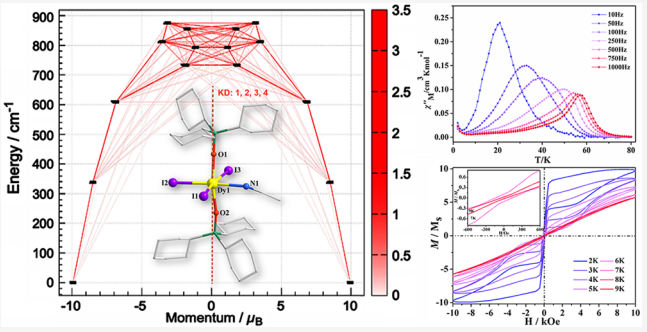

INTRODUCTION

Single-molecule magnets (SMMs), which exhibit slow relaxation of magnetization at the molecular level,[1,2] are expected to be the smallest storage units and quantum objects, invoking intense research interest in the field of spintronic devices and quantum computing.[3−6] The recent fast advances of lanthanides, especially Kramer's Dy^{III} ions, continues to prove the most promising candidates for the design of extraordinary SMMs by virtue of its pronounced magnetic anisotropy.[7−10] One of the most exciting examples is the recent record discovery that Dy^{III} metallocenium cations exhibit hysteresis at close to the temperature of liquid nitrogen and large energy barriers.[11−14] In spite of their exceptional magnetic behavior, however, such a system is not well suited to be processed on functionalized surfaces, given its positive charge and high reactivity.[15,16] A pursuit of practical applications still requires continuous exploitation of new paradigms geared toward the neutral complex which combined a high magnetic anisotropy with a good stability.[17]

Guided with the elegant electrostatic model, the ground state of Dy^{III} ion possessing oblate electron density is expected to be stabilized by the strong axial crystal-field (CF) environments.[18] A linear two-coordinate ligand environment around Dy^{III} is theoretically predicted to be the most superior SMM performance which elicits large level splitting and strong uniaxiality with the relaxation via the highest M_J state.[19−21] Whereas in the axial complexes with higher coordination numbers (CNs) such as the bipyramidal geometry ones, their axiality and the magnitude of energy level splitting depend on the excess extent of the electrostatic repulsion from two atoms in the axial positions over that from the equatorial atoms.[20] It is noteworthy that the increase of ligand ligation tending to occupy equatorial positions would inevitably lead to the decline of CF splitting and increases of the transverse ligand field. A moderate CN should be taken into account to counterbalance the magnetic anisotropy and the stability of Dy^{III} species. Seven-coordinate complexes, possessing oblate Dy^{III} ions in a D_{5h} symmetry, proved good systems that exhibit high effective energy barrier, moderate blocking temperature, and good stability.[22−27] From these geometries, the decrease of the in-plane CNs (i.e., octahedral or trigonal bipyramid architectures) combined with extremely weak donors contributes to a reduction of the transverse CF, which may lead to Dy^{III} complexes with ideally pure M_J states and significant improvement in uniaxial magnetic anisotropy. Among, the six-coordinate complex, with the usually normal CN, is the limiting case to obtain stable low-coordinate Dy^{III} SMMs.[28−32]

Received: February 26, 2020
Published: May 3, 2020

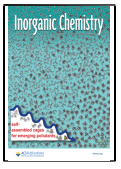

https://dx.doi.org/10.1021/acs.inorgchem.0c00616
Inorg. Chem. 2020, 59, 7158–7166

Besides, the weak nonaxial ligands are expected to be symmetrically disposed on a regular polygon to suppress transverse CF components.[33] Nevertheless, it is not easy to engineer a six-coordinate Dy^{III} complex possessing a highly axial CF, which requires the employment of bulky ligands to force an oblate coordination environment by steric hindrance and geometrical constraints. Among the limited attention paid in the development of six-coordinate Ln^{III} complex, one representative example is an organometallic Dy^{III} bis-(methanediide),[33] where strong axial (C═Dy═C) and weak equatorial (Dy−N) ligand field combined with an axially symmetric equatorial potential results in a high barrier exceeding 700 K and a magnetic blocking temperature up to 10 K. However, high chemical activity toward oxygen and moisture and negative charge characteristics of the complex cannot be ignored. Moreover, Giansiracusa et al. elaborately used the DiMeQ ligand to prepare an air-stable six-coordinate Dy^{III} SMMs with a high energy barrier of ca. 1100 K,[28] exceeding most of the reported seven-coordinate complexes, while there is no hysteresis observed for its pure sample. It is therefore, necessary to carry out more studies of six-coordinate Dy^{III} SMMs as there is a current paucity of examples.

Noting that iodine ion is a big anion, provides diffuse valence orbitals with quite a long metal−ligand bond of ca. 3.0 Å, and owns the electrostatic driving force coordinated with the metal center.[34,35] We attempt to employ them to stabilize near-linear Dy^{III} phosphine oxide architecture. Herein, two equatorial iodide-supported six-coordinate Dy^{III} SMMs, $[Dy(Cy_3PO)_3I_3]\cdot 2THF$ (**1**) and $[Dy(Cy_3PO)_2I_3CH_3CN]$ (**2**) (Cy_3PO = tricyclohexylphosphine oxide), were isolated in a distorted octahedral architecture. Both complexes are charge-neutral molecules and possess a certain degree of stability. Complex **2** achieves a highly axial CF which leads to thermal relaxation via the third excited state pushing the energy barrier to 1062 K and hysteresis loops open up to 9 K. While substitution of the transverse CH_3CN molecule by a strong Cy_3PO ligand on the Dy^{III} site led to the magnetic relaxation of **1** dominated by a Raman process instead of the thermally activated QTM (TA-QTM) process. This work highlights the vast potential of the minimization of transverse ligand field in quickly approaching quantum mechanical limits of anisotropy.

EXPERIMENTAL SECTION

Materials and Measurements. All experiments and manipulations were performed under a dry nitrogen atmosphere using the standard Schlenk techniques or in a glovebox. DyI_3, YI_3, and Cy_3PO was purchased from Alfa Aesar. Toluene and tetrahydrofuran were dried with over sodium under nitrogen atmosphere and distilled twice before use. Hexane was purchased from Adamas and distilled over sodium hydride. Acetonitrile was distilled over calcium oxide under a dinitrogen atmosphere. All dried solvents were stored on activated molecular sieves and/or in K mirrored ampules. Elemental analysis (C, H and N) was carried out on a Perkin Elmer 2400 CHN elemental analyzer. The heat-flow data was recorded by calorimetry measurement using a microcalorimeter of Tian-Calvet type (C80 from Setaram) at a constant temperature of 35 °C in air atmosphere. About 0.1 g of the powder crystalline samples were used. Thermogravimetric analysis (TGA) curves were measured using a NETZSCH STA 449F3 thermal analyzer at a heating rate of 5 °C min^{-1} from 20 to 800 °C with a N_2 atmosphere. The luminescence spectra were recorded using a Horiba-Jobin Yvon Fluorolog-3 luminescence spectrometer, equipped with an Oxford Instruments helium flow optical cryostat. Magnetic susceptibility measurements were collected using a Quantum Design MPMS-XL7 SQUID magnetometer with 1000 Oe applied field in the temperature range of 2−300 K. Alternating current (ac) measurements were performed on the same magnetometer at ac frequencies ranging from 1 to 1000 Hz using a 2.0 Oe oscillating ac field. The samples of magnetic measurements were prepared in the glovebox by loading the samples with multiple recrystallization in an NMR tube and were restrained in eicosane. The samples were then placed under vacuum and flame-sealed. The measured susceptibilities were corrected for the diamagnetism of the constituent atoms and gelatin capsule by using tabulated Pascal constants and the blank sample holders.

Synthesis of $[Dy(Cy_3PO)_3I_3]\cdot 2THF$ (1). A mixture of Cy_3PO (0.444g, 1.5 mmol) and anhydrous DyI_3 (0.272 g, 0.5 mmol) were dissolved in toluene (20 mL). The reaction mixture was refluxed for 10 h, cooled down to room temperature, and filtered. All the volatiles were removed under reduced pressure, and the residue was extracted with THF (30 mL). The extract was filtered, concentrated, and stored at −20 °C freezer overnight to give **1** as yellow crystals (0.646 g, 82% yield). The complex was found to be oxygen- and moisture-stable for at least 1 week in air (Figures S1 and S2). IR (KBr, cm^{-1}): 2930 (s), 2853 (s), 2342 (w), 1630 (w), 1447 (m), 1296 (w), 1216 (w), 1179 (w), 1094 (s), 1044(w), 1005 (w), 893 (w), 856 (w), 763 (w), 733 (w), 694 (w), 565 (w), 548 (w), 532 (w). Anal. Calcd: C, 47.23; H, 7.35. Found: C, 47.01; H, 7.14. Furthermore, the sample after the magnetic measurement was also elemental analyzed. The element content remains almost unchanged suggesting that the THF remains in the lattice for **1** after exposure to vacuum.

Synthesis of $[Dy(Cy_3PO)_2I_3(CH_3CN)]$ (2). A mixture of Cy_3PO (0.296 g, 1 mmol) and anhydrous DyI_3 (0.272 g, 0.5 mmol) was dissolved in acetonitrile (20 mL). The reaction mixture was stirred at room temperature for 48 h, allowed to settle, and then filtered. The extract was concentrated and stored at −20 °C freezer overnight to afford yellow crystals of **2** (0.459 g, 78% yield). The complex was found to be oxygen- and moisture-stable for at least 1 week in air (Figures S1 and S2). Anal. Calcd: C, 45.28; H, 6.97; N, 1.18. Found: C, 45.56; H, 6.75; N, 1.21. IR (KBr, cm^{-1}): 2930 (s), 2853 (s), 2293 (w), 2243 (w), 1628 (m), 1447 (m), 1296 (w), 1217 (w), 1178(w), 1093 (s), 1043 (w), 1006 (w), 918 (m), 893 (m), 856 (w), 763 (w), 648 (m), 566 (w), 548 (m), 532 (m), 455 (w).

Synthesis of Dysprosium-Doped Yttrium Samples 1@Y and 2@Y. Two magnetically diluted samples were generated by accurately mixing DyI_3 and YI_3 in a 1:19 molar ratio, following the same procedure described as **1** and **2**, respectively. The final crystalline product with final ratios of Dy/Y 1:16.42 for **1** and 1:15.65 for **2** was determined by the ICP-OES 730.

X-ray Single-Crystal Diffraction Analysis. Single-crystal X-ray data for complexes **1** and **2** were collected on a Bruker Smart Bruker APEX II CCD diffractometer with a Mo Kα X-ray source (Kα = 0.71073 Å) at 120 K using an Oxford Cryosystems Cobra low-temperature device. Cell determination and data reduction were processed with the SAINT processing program.[36] The absorption correction based on multiscan was applied in SADABS.[37] By using Olex2,[38] the structures were solved by direct methods with SHELXT and refined by full-matrix least-squares techniques against F^2 using SHELXL-2014 programs.[39] The SQUEEZE subroutine of the PLATON software was used to remove the scattering from the highly disordered solvent molecules.[40] The resulting new HKL files were used to further refine the structures. All non-hydrogen atoms were refined anisotropically. All hydrogen atoms were placed in calculated positions and refined isotropically. The crystal data and structural refinement parameters are summarized in Table S1, while selected bond lengths and angles for complexes **1** and **2** are listed in Table S2.

RESULTS AND DISCUSSION

Structural Characterization. Complex **1** crystallizes in the triclinic system with space group $P\bar{1}$, while **2** belongs to the orthorhombic space group *Pbca* (Table S1). The Dy^{III} center of two complexes is found to be six-coordinated with an octahedron geometry, where the axial positions are occupied by two *trans*-phosphoryl oxygens from Cy_3PO ligands, while

https://dx.doi.org/10.1021/acs.inorgchem.0c00616
Inorg. Chem. 2020, 59, 7158−7166

the equatorial planes are completed by three I^- ions and either one neutral Cy_3PO (**1**) or CH_3CN (**2**) molecule (Figure 1).

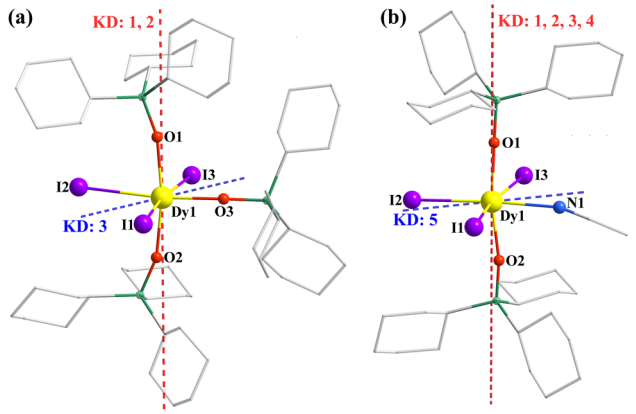

Figure 1. Molecular structure of complexes **1** (a) and **2** (b). Hydrogen atoms are omitted for clarity. For unlabeled atoms: P, green, and C, gray. Dashed lines represent the magnetic axis in the ground and excited KDs of these complexes determined by the *ab initio* calculations.

The continuous shape measures show a slightly more distorted coordination polyhedron for **1** (Table S3).[41] The axial Dy−O distances are 2.212(4) Å for **1** and 2.1760(14)/2.1844(14) Å for **2**, whereas the equatorial Dy−I distances are obviously much longer in the range 3.0549(5)−3.0974(6) Å for **1** and 2.9886(3)−3.0595(3) Å for **2**. Another equatorial single-coordinated Dy−O bond length is 2.223(4) Å for **1** and Dy−N bond length is 2.5018(18) Å for **2** (Table S2). The axial O−Dy−O angle is near-linear at 170.51(15)° for **1** and 170.21(5)° for **2**. Comparatively, the structural difference between **1** and **2** is reflected mainly in equatorial positions of coordinated Cy_3PO (**1**) or CH_3CN (**2**) ligand, which occupy markedly different Dy−O/Dy−N distances. All bond lengths of equatorial plane in **2** are long (above 2.5 Å), and the average equatorial distance is up to 2.891 Å. The resultant crystal fields of **1** and **2** are assessed by *ab initio* studies (*vide infra*). Within the lattice, the neighboring Dy sites of complex **1** run parallel related by inversion center symmetry, leading to the shortest Dy···Dy separations of 11.013 Å (Figure S3). For **2**, the unit cell contains eight molecules with a shorter Dy···Dy distance of 9.654 Å (nearest neighbors), and these molecules are connected by the greater number of symmetry operations including screw, inversion and glide (Figure S4). The presence of screw (2_1) symmetries around three Cartesian axes induces different molecular orientations, providing local fluctuating transverse magnetic fields associated with increased tunneling rates.

Stability Analysis. The chemical and thermal stability of **1** and **2** are evaluated using heat flux data measured by a C80 microcalorimeter in air atmosphere and thermogravimetric analysis (TGA) curves carried out in a N_2 flow, respectively (Figure S1 and S2). The heat flux curves of **1** and **2** show that no any heat exchange (endothermic or exothermic process) takes places at 1 week, indicating that there are no deliquescence or chemical changes for complexes **1** and **2**. Elemental analyses (C, H, and N) of the samples after thermal analysis were detected again (Found: C, 46.93; H, 7.21, for **1**; Found: C, 45.66; H, 6.82; N, 1.31, for **2**), further proving the chemical stability toward oxygen and moisture for these molecules. The TGA curve of **1** indicates an initial weight loss of 4.69% below 95 °C, corresponding to the loss of two tetrahydrofuran molecules in the lattice (calcd 4.57%). For **2**, about 3.22% weight loss is observed from 150 to 230 °C, which corresponds to the coordinated acetonitrile molecules leaving (calcd 3.48%). The framework begins to decompose after being heated over 300 °C.

Static and Dynamic Magnetic Properties. Direct current (dc) magnetic susceptibilities of **1** and **2** were collected between 300 and 2 K with an applied field of 1 kOe (Figures S5 and S6). The room-temperature $\chi_M T$ values are determined to be 14.09 and 13.95 $cm^3\ mol^{-1}\ K$ for **1** and **2**, respectively, close to the expected value of 14.17 $cm^3\ mol^{-1}\ K$ for one Dy^{III} ion ($^6H_{15/2}$, g = 4/3). Upon lowering the temperature, both complexes experience slowly decrease of $\chi_M T$ product as a result of depopulation of the M_J levels. Further cooling results in a precipitous drop in $\chi_M T$ curves below 10 K, suggestive of magnetic blocking. Consistently, the field-cooled (FC) and zero-field-cooled (ZFC) magnetization data recorded for **1** and **2** give divergences at ca. 4 and 7.4 K, respectively, verifying blocking of the molecular spin (Figure S7). While the magnetization curves below 20 K show a sharp increase at low magnetic fields without any saturation above 5 T, implying well-separated excited-energy levels for Dy^{III} ions (Figure S8).

The dynamics of the magnetization were determined by alternating current (ac) susceptibility measurements at zero dc field. Complexes **1** and **2** exhibit the slow relaxation of magnetization up to 20 and 60 K, respectively, but clear overlapping peak maxima in χ'' (ν) and increase of $\chi''(T)$ at low temperatures are observed suggesting the presence of a QTM regime (Figures 2a, 3a, and S9−S12). Such a QTM effect is further minimized upon an applied optimal dc field of

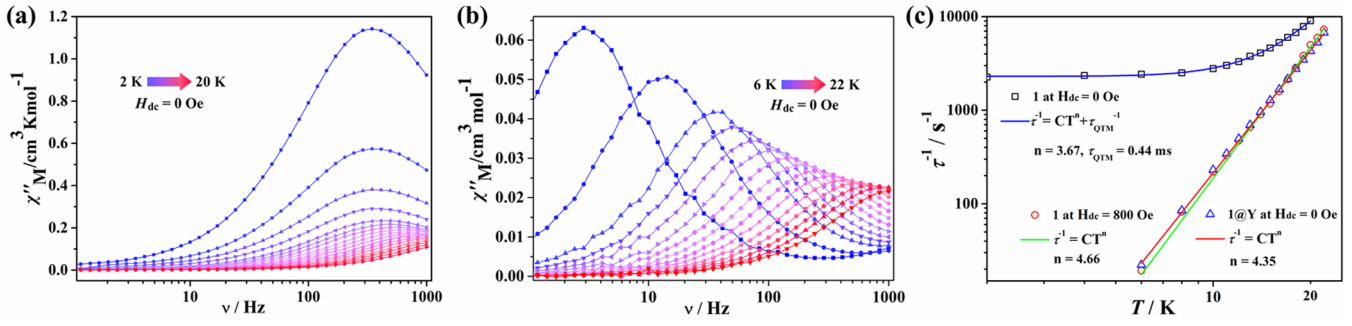

Figure 2. Frequency-dependent out-of-phase χ'' ac susceptibility signals for **1** (a) and **1@Y** (b) at zero static field. Temperature dependence of the relaxation time τ in zero (blue) and 800 Oe dc fields (red) for **1** and for **1@Y** (pink) (c). The solid lines represent the best fit.

https://dx.doi.org/10.1021/acs.inorgchem.0c00616
Inorg. Chem. 2020, 59, 7158−7166

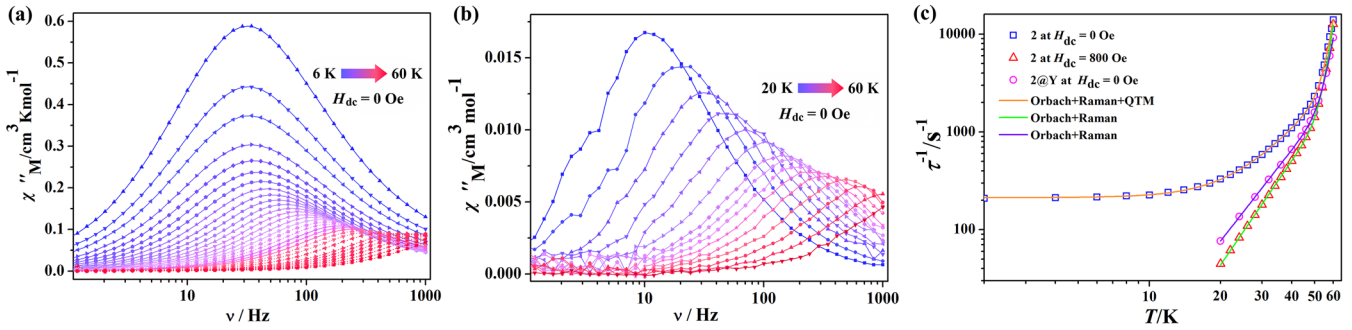

Figure 3. Frequency-dependent out-of-phase χ'' ac susceptibility signals for **2** (a) and **2@Y** (b) at zero static field. Temperature dependence of the relaxation time τ in zero (blue) and 800 Oe dc fields (red) for **2** and for **2@Y** (pink) (c). The solid lines represent the best fit.

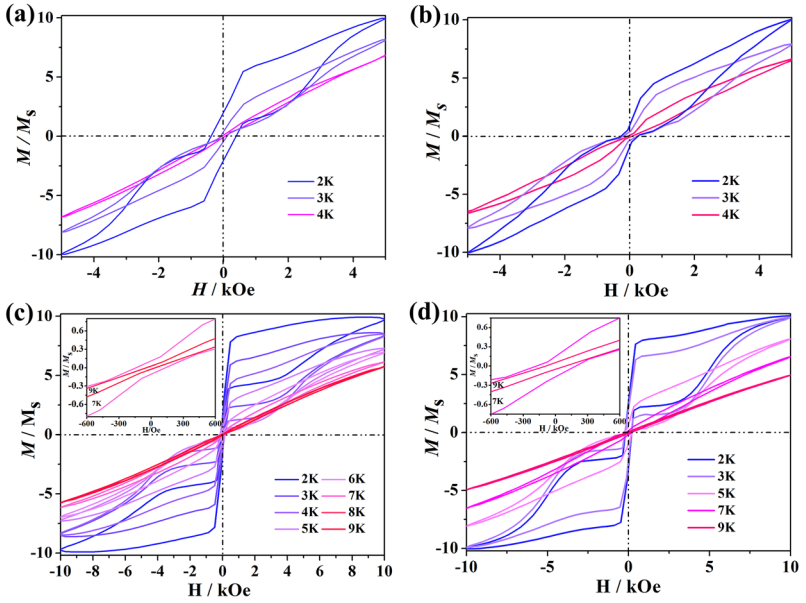

Figure 4. *M* vs *H* hysteresis profiles of **1** (a), **1@Y** (b), **2** (c), and **2@Y** (d), with a magnetic field sweep rate of 18 mT s^{-1}. Inset: enlargement of the 7 and 9 K signals at small field.

800 Oe (Figures S13–S17). The relaxation times τ of **1** and **2** are extracted by the generalized Debye model using CC-FIT program (Figures S18 and S19).[42] A moderate relaxation times distribution (α) of 0.051–0.19 (2–20 K) for **1** and 0.013–0.22 (2–60 K) for **2** at H_{dc} = 0 and narrower distribution of 0.052–0.098 (6–22 K) for **1** and 0.010–0.020 (20–60 K) for **2** in H_{dc} = 800 Oe are obtained (Tables S4–S7).

Providing further insight into the relaxation dynamics of **1**, the relaxation rate in zero dc field shows the markedly temperature-dependent at high temperature and gradual leveling at low temperature (T < 8 K), correlating to a QTM regime (Figure S20). Treating the high-temperature data with a power law ($\tau^{-1} = CT^n$) gives a small n value of 2.3 above 14 K, suggesting the dominant Raman process rather than the TA-QTM behavior in high temperature (Figure S20). Thus, the best fitting of the τ^{-1} versus T plot including tunneling and Raman term, namely, $\tau^{-1} = CT^n + \tau_{QTM}^{-1}$, gives n = 3.67, C = 0.11, and τ_{QTM} = 0.44 ms (Figure 2c). This Raman behavior is still the preferential relaxation channel for the ac data in a 800 Oe dc field as suggested by the almost perfect linear trend of $\log(\tau^{-1})$ versus $\log(T)$, which can be fitted by a solely Raman term with n = 4.66. Furthermore, an attempt to include an activation mechanism instead of the Raman one gives an estimation of the "apparent energy barrier" in the high-temperature range U_{app} = 69 K (0 Oe) and 84 K (800 Oe), far from the calculated energy of the first excited state (282.5 cm^{-1}). This is an additional evidence for the dominant Raman relaxation in **1** instead of an TA-QTM process.

On the contrary, the ac susceptibility data for **2** reveal much longer relaxation times (Figure 3c). The temperature dependence of the relaxation rate shows an exponential profile above 50 K suggesting the dominant TA-QTM contribution at high temperatures for **2**. At lower temperatures, the log–log plots of τ^{-1} versus T are gradually linear associated with a Raman component. Then, a near temperature-independent QTM regime is reached below 10 K in zero dc field, a feature that is not observed on the time scale of ac measurement for the optimal dc field (Figure 3c). A fit of the data in H_{dc} = 0 and 800 Oe (assuming $\tau_{QTM}^{-1} = 0$) were therefore simultaneously considered using eq 1:

$$\tau^{-1} = \tau_{QTM}^{-1} + CT^n + \tau_0^{-1} \exp(-U_{eff}/k_BT) \quad (1)$$

The best fit for **2** yields the parameters of U_{eff} = 1002 K (697.1 cm^{-1}), $\tau_0 = 5.0 \times 10^{-12}$ s, C = 0.017 s^{-1} K$^{-2.95}$, n = 2.95, and τ_{QTM} = 4.7 ms under H_{dc} = 0 Oe, while under H_{dc} = 800 Oe, it affords U_{eff} = 1078 K (749.4 cm^{-1}), $\tau_0 = 1.55 \times 10^{-12}$ s, C =

https://dx.doi.org/10.1021/acs.inorgchem.0c00616
Inorg. Chem. 2020, 59, 7158–7166

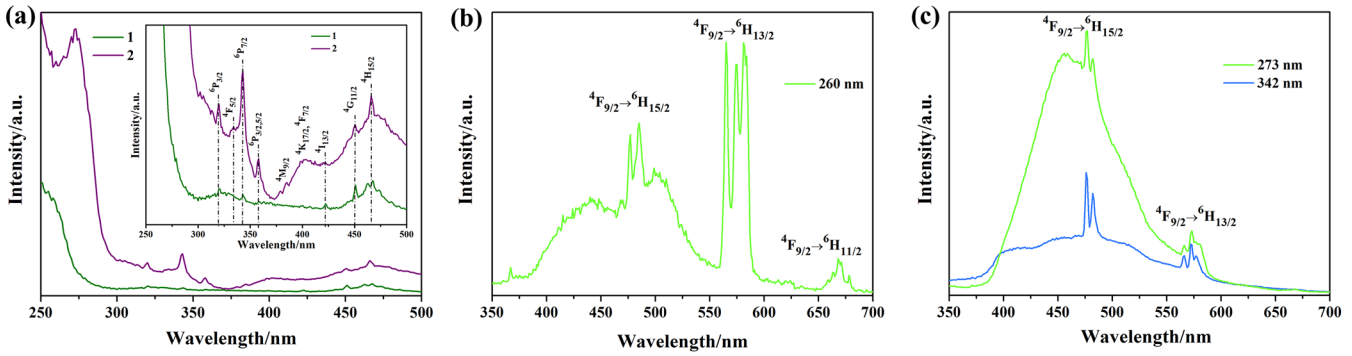

Figure 5. Excitation spectra of complexes **1** and **2** at 10 K and monitored at 573 nm. Inset: magnification of excitation spectra to identify intra-4f self-absorptions (a). Luminescence spectra of complexes **1** excited at 260 nm (b) and **2** excited at 273 and 342 nm at 10 K (c).

Table 1. *Ab Initio* Calculated Spin-Orbital Energies, Corresponding *g* Tensors, Angles of the Main Magnetic Axes Relative to the Main Magnetic Axis of the Ground State and Crystal Field Wave Function for the Five Kramer Doublets (KDs) of the $^6H_{15/2}$ Ground Multiplet of Dy^{III} in 2

KDs	spin−orbit energies (cm^{-1})	*g*			g_z angle (deg)	crystal field wave function
		g_X	g_Y	g_Z		
1	0.0	0.00086	0.0010	19.8764	0	$>99\%\left\vert\pm\frac{15}{2}\right\rangle$
2	338.6	0.02504	0.0306	17.0127	0.89	$>99\%\vert\pm 132\rangle$
3	608.6	0.5788	0.7728	13.7351	2.62	$94\%\left\vert\pm\frac{11}{2}\right\rangle$
4	732.8	10.1060	8.1193	3.6422	4.81	$28\%\vert\pm 92\rangle + 65\%\vert \pm 12\rangle$
5	793.5	1.8897	4.4994	12.1220	83.88	$21\%\vert\pm 52\rangle + 70\%\vert\pm 32\rangle$

$0.0011\ s^{-1}\ K^{-3.54}$, and $n = 3.54$. Clearly, the ligand field of CH_3CN is weaker than Cy_3PO facilitating the more compressed axial CF and slower relaxation through thermal mean for **2**.

Also, the influence of intermolecular dipole interactions is studied by the magnetic site dilution. A relaxation behavior of zero-field data for diluted samples (5% **1@Y** and 5% **2@Y**) can be found that is similar to their concentrated samples at the optimal dc field, confirming the molecular origin of SMM behavior in investigated complexes (Figures 2b,c and 3b,c, Tables S8 and S9). A full fitting of the relaxation data of **2@Y** by considering Orbach (U_{eff} = 1062 K (738.5 cm^{-1}), $\tau_0 = 2.56 \times 10^{-12}$ s) and Raman ($C = 0.0065\ s^{-1}\ K^{-3.13}$, $n = 3.13$) gives a similar energy barrier to the pure complex indicating the dominant TA-QTM process in high-temperature relaxation, in contrast to **1@Y** for which Raman mechanism are still largely operative (Figure 2c). Noticeably, the disappearance of temperature-independent quantum tunneling in **2@Y** suggests that the rapid QTM in the concentrated sample is appreciably assisted by the dipolar interactions from the neighboring spins. The different oriented arrangement of molecules in the lattice of **2** is most likely responsible for the dipolar origins even if the nearest neighboring Dy···Dy distance is as large as 9.654 Å (Figure S4).

Magnetic Hysteresis. Magnetic hysteresis is clearly observed in $M(H)$ loops for both **1** and **2** to at least 4 and 9 K, respectively, for a sweep rate of 18 mT s^{-1} (Figure 4a,c), but the characteristic significant step of butterfly-shaped loops at near-zero field strongly limit an observation of large coercivity due to the strong tunneling rate at low fields. On measuring the magnetic site dilution samples of the molecule, the slightly larger opening is well-observed, indicating a single-ion nature of magnetization for both complexes (Figure 4b,d). It is also noted, however, that the zero-field drop in hysteresis is not completely removed by the magnetic site dilution; thus, the internal dipolar field is not the sole cause to facilitate QTM. Hyperfine coupling and/or low ligand field symmetry may also contribute to tunneling pathways.[43,44]

Photoluminescence Studies. The photoluminescence measurements for two Dy^{III} complexes were carried out at 10 K to correlate with the magnetic results. The excitation spectra of the samples by monitoring the Dy^{III} $^4F_{9/2} \rightarrow {}^6H_{13/2}$ transition at 573 nm reveal a series of weak f−f self-absorptions and an intense broad band before 300 nm which dominates the excitation spectrum, pointing out that the main excitation path for the Dy^{III} ions is through the ligand, rather than direct population of the f−f levels (Figure 5a). Excitation of **1** at 260 nm shows three groups of characteristic emission peaks of Dy^{III} ions at around 480, 575, and 670 nm, corresponding to the $^4F_{9/2} \rightarrow {}^6H_{15/2,13/2,11/2}$ transitions, respectively (Figure 5b), whereas these characteristic peaks are superimposed with the ligand-related broad band centered at about 415 and 525 nm. This behavior is more prominent in **2**, whose characteristic $^4F_{9/2} \rightarrow {}^6H_{15/2,13/2}$ transition of Dy^{III} ions are strongly influenced by the broad band in the range of 390−470 nm and 490−560 nm with monitoring at either the ligand (273 nm) or direct intra-4f excitation (342 nm), as displayed in Figure 5c. The intensity of the $^4F_{9/2} \rightarrow {}^6H_{13/2}$ transition (the yellow emission) in **1** is stronger than that of the $^4F_{9/2} \rightarrow {}^6H_{15/2}$ (the blue emission); conversely, a blue emission at 475 nm is much stronger in **2**. These behaviors suggest that the ligands in **1** and **2** are suitable for the sensitization of different wavelength luminescence of Dy^{3+}. However, the large broadness of the $^4F_{9/2} \rightarrow {}^6H_{15/2}$ transitions in **1** and **2** prohibit any unambiguous extraction of CF splitting energies for the ground

https://dx.doi.org/10.1021/acs.inorgchem.0c00616
Inorg. Chem. 2020, 59, 7158−7166

states and the excited multiplets for comparison with the experimental and theoretical results.

Theoretical Analysis. *Ab initio* calculations of the CASSCF/RASSI/SINGLE_ANISO type with MOLCAS 8.3 have been performed on **1** and **2** to further understand the differences in the local electronic structure and their magnetic behaviors (see the Supporting Information for details).[45,46] The Dy^{III} sites on complexes **1** and **2** show a pure $M_J = \pm 15/2$ ground state, and the ground state *g*-tensor is highly axial (g_x = 0.0017, g_y = 0.0030, g_z = 19.8538 and g_x = 0.00086, g_y = 0.0010, g_z = 19.8764) followed with small but non-negligible transverse components, which explains the observed zero-field SMM behavior (Tables 1, S11, and S13). A large energy separation between the lowest and first excited states of about 280−340 cm^{-1} is predicted. The main magnetic axes in the ground KD of **1** and **2** are found to be of nearly identical directions, that is, closing to the orientation along the apical two phosphine oxide ligands (Figure 1). However, it can be noted that the magnetic axiality in **2** is higher than **1**. Focusing on **2**, the wave function of the three lowest energy KDs is almost of pure $|\pm 15/2\rangle$, $|\pm 13/2\rangle$, and $|\pm 11/2\rangle$ types, with a significant mixing in the subsequent fourth states (Table 1). Correspondingly, the main magnetic axes of the ground KD to the third excited KD in **2** are almost collinear (with the maximum tilt of 4.81° from the ground KD), as shown in Figure 1. For **1**, the presence of an equatorially coordinated Cy_3PO ligand greatly lowers the magnetic axiality in the excited KDs: The first excited KD of **1** has larger transversal components ($g_{x,y} \approx 10^{-1}$) and is mainly M_J $|\pm 13/2\rangle$ state (0.92). The higher excited states, however, are found to own the obviously raised $g_{x,y}$ tensors, and the wave functions are strongly mixed (Tables S11 and S13). Moreover, the *ab initio* calculated CF parameters point out that the axial parameters of $B(2, 0)$, $B(4, 0)$, and $B(6, 0)$ in **2** are 1 order of magnitude larger than in **1**, explaining the higher degree of axiality and the larger CF splitting in **2** (Table S15).

The blocking barrier of the investigated complexes are also presented in Figure 6. Associated with the calculated transition matrix elements of the magnetization, it is found that the QTM components in the ground and first excited KDs for **2** are negligible ($0-10^{-3}$ μ_B), and the TA-QTM components at the $M_J = \pm 11/2$ state is still minimized (0.225 μ_B) (Table S16). As a result, the most probable relaxation pathway involves the third excited state with an energy barrier of 732.8 cm^{-1}. The computational barrier heights are in good agreement with the ones extracted from the ac susceptibility data (697 cm^{-1} for a pure sample and 738 cm^{-1} for a diluted sample). In contrast, for **1**, the transversal *g*-factors in the first excited state ($M_J = \pm 13/2$) already become quite large (Table S11), and the thermal relaxation most likely proceeds via this state. Actually, we obtained a much smaller experimental "barrier" (48 cm^{-1} at H_{dc} = 0 Oe and 58 cm^{-1} at H_{dc} = 800 Oe) than the calculated energy of the first excited state (292.5 cm^{-1}). The additional account of the dynamical correlation using the Extended Multistate (XMS) CASPT2 method for a reduced structural fragment of **1** (Figures S25 and S26) essentially confirms the CASSCF results (Tables S18 and S19 and Figures S27−S32).[48] This is additional evidence for the dominant Raman relaxation process in **1** within the investigated temperature domain. Actually, the temperature-assisted QTM via the first excited state certainly contributes to the total relaxation rate. However, this contribution is negligible in the investigated temperature domain and is expected to become dominant at 30−50 K. Large differences in the magnetic behavior for **1** and

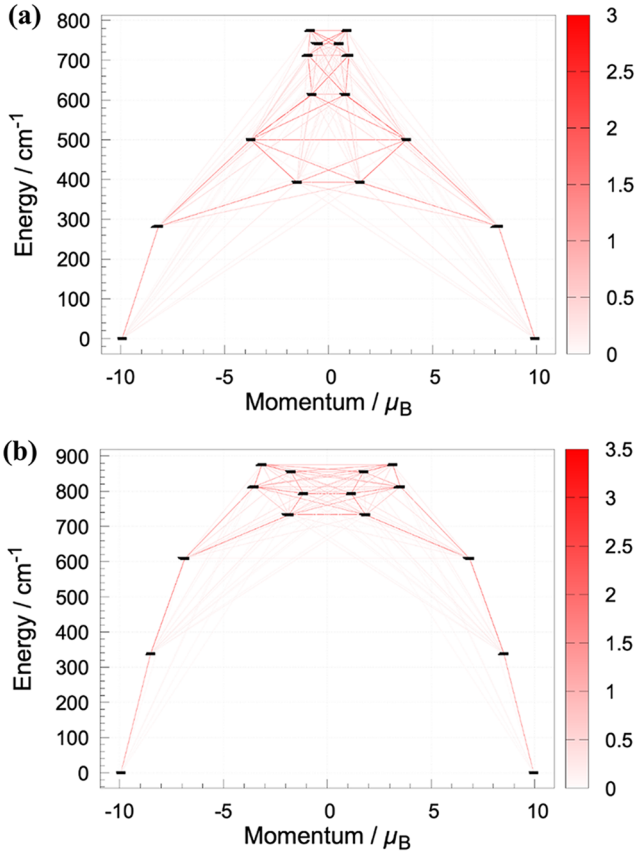

Figure 6. Magnetization blocking barrier for **1** (a) and **2** (b). Each doublet state $\pm M_J$ arising from a given atomic multiplet $^{2S+1}L_J$ is placed according to its saturation magnetic moment (horizontal axis). The intensity of the pink lines indicates the amplitude of the average transition magnetic dipole moment in μ_B between the connected states (see the legend in the right-hand side), the square of which roughly scales with the rate of spin-phonon transition between them.[47] The most intense lines outline the magnetization blocking barrier (solid red lines).

2 relating with different transverse ligand field intensity point out that the oblate Dy^{III} ion requires a strong axial ligand, but weak ligation at each equatorial site is equally important to ensure the relaxation to be thermally activated.

We were curious about **2**, with a low symmetry structure but showing high KDs purity. Actually, the axial purity of the ground and excited KDs is related to the axiality of the crystal field, in other words, to the ratio between the effects of the axial ligands versus the effect of the equatorial ligands. The reason for the slight nonaxiality of complex **2** is the effect of the equatorial ligands. Iodine seems to behave as a weak ligand, not much affecting the axiality of the central Dy^{III} ion. We assume that the reason for the relatively weak effect of iodine is that this ion is relatively large, and its formal negative charge is delocalized in a large space domain. The same is true about the nitrogen-bonded ligand like pyridine nitrogen seems also a weak ligand, as it is able to form chemical bonds as neutral.

Notably, compared with the other negatively charged oxygen donors, the neutral Cy_3PO ligands may contribute less repulsion to the metal center, as suggested by the relatively long $Dy-O_{phosphine\_oxygen}$ bond lengths, than the anion ones (Table S20). Complex **2** achieves highly axial CF and is the first single-ion magnet that uses the neutral ligands dominate

https://dx.doi.org/10.1021/acs.inorgchem.0c00616
Inorg. Chem. 2020, 59, 7158−7166

the anisotropic barriers exceeding 1000 K. It is also one of the few examples where the energy barrier and the hysteresis opens are remarkable in the O_h coordination environment (Table S21). Compared with other phosphine oxide based Dy^{III} single-ion magnet featuring five water molecules in the equatorial plane,[23−25,49,50] **2** exhibits the highest energy barrier (1062 K), the highest efficient relaxation pathways (the third excited state), and the highest ac peak temperature (58 K at 1000 Hz). The appreciably enhanced relaxation behavior of **2** mainly benefits from the efficient reduction of the ligand field strength and the coordination number of equational donors, allowing the Dy^{III} ion to easily maintain highly uniaxial magnetic anisotropy in an appropriate axial ligand field environment, while the relatively small magnetic hysteresis of **2** would likely be associated with a dominant Raman relaxation and QTM. In addition, it is worth noting that the magnetic properties of **2** are comparable to those of the recent major breakthrough of two types of Dy^{III} complexes with D_{5h} and D_{6h} symmetry.[22,27,51,52] This implies that there are various coordination geometries available to implement the strong axial CF.

CONCLUSIONS

To summarize, we reported two neutral equatorial iodide-supported octahedral Dy^{III} SMMs, $[Dy(Cy_3PO)_3I_3]\cdot 2THF$ (**1**) and $[Dy(Cy_3PO)_2I_3CH_3CN]$ (**2**) with a certain degree of stability. Relying on one of the laterally different Cy_3PO (**1**) or CH_3CN (**2**) coordination, the opposite mechanism of relaxation for the two complexes was observed. Notably, **2** exhibits a highly axial CF with a U_{eff} of 1062 K and hysteresis loops open up to 9 K. The observed U_{eff} larger than 1000 K in the system of natural ligands dominated the anisotropy undoubtedly highlight the importance of the minimization of transverse ligand field in improving the SMMs properties. However, the observed axiality and stability for the complex here are far from meeting the demands for practical applications, but it is clearly proved that the highly axial six-coordinate lanthanide system can mutual balance two necessary factors. Under the current situation of approaching the available limits of strong coordination bond, the reduction of the transverse ligand field to promote higher axiality of Ln^{III} provides an available path toward high-performance SMMs.

ASSOCIATED CONTENT

Supporting Information

The Supporting Information is available free of charge at https://pubs.acs.org/doi/10.1021/acs.inorgchem.0c00616.

Crystal data and structures; stability characterization; magnetic measurements; details of *ab initio* calculations; table for the comparison of magneto-structural correlations (PDF)

Accession Codes

CCDC 1887053−1887054 contain the supplementary crystallographic data for this paper. These data can be obtained free of charge via www.ccdc.cam.ac.uk/data_request/cif, or by emailing data_request@ccdc.cam.ac.uk, or by contacting The Cambridge Crystallographic Data Centre, 12 Union Road, Cambridge CB2 1EZ, UK; fax: +44 1223 336033.

AUTHOR INFORMATION

Corresponding Authors

Zhengqiang Xia − *Key Laboratory of Synthetic and Natural Functional Molecule Chemistry of Ministry of Education, College of Chemistry and Materials Science, Northwest University, Xi'an 710127, China;* orcid.org/0000-0002-9342-8422; Email: northwindy@126.com

Liviu Ungur − *Department of Chemistry, National University of Singapore, 117543, Singapore;* orcid.org/0000-0001-5015-4225; Email: chmlu@nus.edu.sg

Dan Liu − *Institute of Flexible Electronics (IFE), Northwestern Polytechnical University (NPU), Xi'an 710072, China;* Email: iamdliu@nwpu.edu.cn

Sanping Chen − *Key Laboratory of Synthetic and Natural Functional Molecule Chemistry of Ministry of Education, College of Chemistry and Materials Science, Northwest University, Xi'an 710127, China;* orcid.org/0000-0002-6851-7386; Email: sanpingchen@126.com

Authors

Min Li − *Key Laboratory of Synthetic and Natural Functional Molecule Chemistry of Ministry of Education, College of Chemistry and Materials Science, Northwest University, Xi'an 710127, China*

Haipeng Wu − *Key Laboratory of Synthetic and Natural Functional Molecule Chemistry of Ministry of Education, College of Chemistry and Materials Science, Northwest University, Xi'an 710127, China*

Liviu F. Chibotaru − *Theory of Nanomaterials Group and Institute of Nanoscale Physics and Chemistry -INPAC, Katholieke Universiteit Leuven, 3001 Leuven, Belgium*

Hongshan Ke − *Key Laboratory of Synthetic and Natural Functional Molecule Chemistry of Ministry of Education, College of Chemistry and Materials Science, Northwest University, Xi'an 710127, China*

Shengli Gao − *Key Laboratory of Synthetic and Natural Functional Molecule Chemistry of Ministry of Education, College of Chemistry and Materials Science, Northwest University, Xi'an 710127, China*

Complete contact information is available at: https://pubs.acs.org/10.1021/acs.inorgchem.0c00616

Author Contributions

‖M.L. and H.W. contributed equally to this work.

Notes

The authors declare no competing financial interest.

ACKNOWLEDGMENTS

We gratefully acknowledge financial support from the National Natural Science Foundation of China (grant nos. 21673180, 21727805, 21803042, and 21973074), the Natural Science Basic Research Program of Shaanxi (grant nos. 2017JZ002, 2018JM5180, and 2019JQ-067), and the 64th China Postdoctoral Science Foundation Funded Project (2018M643706). The scientific grants R-143-000-A80-114 and R-143-000-A65-133 from the National University of Singapore are gratefully acknowledged. Computational resources from NSCC (ASPIRE-1, grant 11001278) were used for this study. D.L. is supported by Natural Science Basic Research Progrom of Shaanxi (program no.2020JQ-136).

REFERENCES

(1) Sessoli, R.; Gatteschi, D.; Caneschi, A.; Novak, M. A. Magnetic bistability in a metal-ion cluster. *Nature* **1993**, *365* (6442), 141−143.
(2) Gatteschi, D.; Sessoli, R.; Villain, J. *Molecular Nanomagnets*; Oxford University Press: Oxford, 2006.
(3) Winpenny, R. E. P. Quantum Information Processing Using Molecular Nanomagnets As Qubits. *Angew. Chem., Int. Ed.* **2008**, *47* (42), 7992−7994.
(4) Pedersen, K. S.; Ariciu, A.-M.; McAdams, S.; Weihe, H.; Bendix, J.; Tuna, F.; Piligkos, S. Toward Molecular 4f Single-Ion Magnet Qubits. *J. Am. Chem. Soc.* **2016**, *138* (18), 5801−5804.
(5) Mannini, M.; Pineider, F.; Sainctavit, P.; Danieli, C.; Otero, E.; Sciancalepore, C.; Talarico, A. M.; Arrio, M.-A.; Cornia, A.; Gatteschi, D.; Sessoli, R. Magnetic memory of a single-molecule quantum magnet wired to a gold surface. *Nat. Mater.* **2009**, *8*, 194.
(6) Affronte, M. Molecular nanomagnets for information technologies. *J. Mater. Chem.* **2009**, *19* (12), 1731−1737.
(7) Harriman, K. L. M.; Errulat, D.; Murugesu, M. Magnetic Axiality: Design Principles from Molecules to Materials. *Trends in Chem.* **2019**, *1* (4), 425−439.
(8) Zhu, Z.; Guo, M.; Li, X. L.; Tang, J. Molecular magnetism of lanthanide: Advances and perspectives. *Coord. Chem. Rev.* **2019**, *378*, 350−364.
(9) Meng, Y. S.; Jiang, S. D.; Wang, B. W.; Gao, S. Understanding the Magnetic Anisotropy toward Single-Ion Magnets. *Acc. Chem. Res.* **2016**, *49* (11), 2381−2389.
(10) Liu, J. L.; Chen, Y. C.; Tong, M. L. Symmetry strategies for high performance lanthanide-based single-molecule magnets. *Chem. Soc. Rev.* **2018**, *47* (7), 2431−2453.
(11) Guo, F.-S.; Day, B. M.; Chen, Y.-C.; Tong, M.-L.; Mansikkamäki, A.; Layfield, R. A. Magnetic hysteresis up to 80 K in a dysprosium metallocene single-molecule magnet. *Science* **2018**, *362* (6421), 1400−1403.
(12) Goodwin, C. A. P.; Ortu, F.; Reta, D.; Chilton, N. F.; Mills, D. P. Molecular magnetic hysteresis at 60 K in dysprosocenium. *Nature* **2017**, *548* (7668), 439−442.
(13) Guo, F.-S.; Day, B. M.; Chen, Y.-C.; Tong, M.-L.; Mansikkamäki, A.; Layfield, R. A. A Dysprosium Metallocene Single-Molecule Magnet Functioning at the Axial Limit. *Angew. Chem., Int. Ed.* **2017**, *56* (38), 11445−11449.
(14) McClain, K. R.; Gould, C. A.; Chakarawet, K.; Teat, S. J.; Groshens, T. J.; Long, J. R.; Harvey, B. G. High-temperature magnetic blocking and magneto-structural correlations in a series of dysprosium(III) metallocenium single-molecule magnets. *Chem. Sci.* **2018**, *9* (45), 8492−8503.
(15) Sessoli, R. Magnetic molecules back in the race. *Nature* **2017**, *548*, 400.
(16) Gould, C. A.; McClain, K. R.; Yu, J. M.; Groshens, T. J.; Furche, F.; Harvey, B. G.; Long, J. R. Synthesis and Magnetism of Neutral, Linear Metallocene Complexes of Terbium(II) and Dysprosium(II). *J. Am. Chem. Soc.* **2019**, *141* (33), 12967−12973.
(17) Studniarek, M.; Wäckerlin, C.; Singha, A.; Baltic, R.; Diller, K.; Donati, F.; Rusponi, S.; Brune, H.; Lan, Y.; Klyatskaya, S.; Ruben, M.; Seitsonen, A. P.; Dreiser, J. Understanding the Superior Stability of Single-Molecule Magnets on an Oxide Film. *Adv. Sci.* **2019**, *6*, 1901736.
(18) Rinehart, J. D.; Long, J. R. Exploiting single-ion anisotropy in the design of f-element single-molecule magnets. *Chem. Sci.* **2011**, *2* (11), 2078−2085.
(19) Chilton, N. F. Design criteria for high-temperature single-molecule magnets. *Inorg. Chem.* **2015**, *54* (5), 2097−2099.
(20) Ungur, L.; Chibotaru, L. F. Strategies toward High-Temperature Lanthanide-Based Single-Molecule Magnets. *Inorg. Chem.* **2016**, *55* (20), 10043−10056.
(21) Chilton, N. F.; Goodwin, C. A. P.; Mills, D. P.; Winpenny, R. E. P. The first near-linear bis(amide) f-block complex: a blueprint for a high temperature single molecule magnet. *Chem. Commun.* **2015**, *51* (1), 101−103.
(22) Liu, J.; Chen, Y. C.; Liu, J. L.; Vieru, V.; Ungur, L.; Jia, J. H.; Chibotaru, L. F.; Lan, Y.; Wernsdorfer, W.; Gao, S.; Chen, X. M.; Tong, M. L. A Stable Pentagonal Bipyramidal Dy(III) Single-Ion Magnet with a Record Magnetization Reversal Barrier over 1000 K. *J. Am. Chem. Soc.* **2016**, *138* (16), 5441−5450.
(23) Chen, Y. C.; Liu, J. L.; Ungur, L.; Liu, J.; Li, Q. W.; Wang, L. F.; Ni, Z. P.; Chibotaru, L. F.; Chen, X. M.; Tong, M. L. Symmetry-Supported Magnetic Blocking at 20 K in Pentagonal Bipyramidal Dy(III) Single-Ion Magnets. *J. Am. Chem. Soc.* **2016**, *138* (8), 2829−2837.
(24) Gupta, S. K.; Rajeshkumar, T.; Rajaraman, G.; Murugavel, R. An air-stable Dy(iii) single-ion magnet with high anisotropy barrier and blocking temperature. *Chem. Sci.* **2016**, *7* (8), 5181−5191.
(25) Canaj, A. B.; Singh, M. K.; Wilson, C.; Rajaraman, G.; Murrie, M. Chemical and in silico tuning of the magnetisation reversal barrier in pentagonal bipyramidal Dy(iii) single-ion magnets. *Chem. Commun.* **2018**, *54* (59), 8273−8276.
(26) Liu, J. L.; Chen, Y. C.; Zheng, Y. Z.; Lin, W. Q.; Ungur, L.; Wernsdorfer, W.; Chibotaru, L. F.; Tong, M. L. Switching the anisotropy barrier of a single-ion magnet by symmetry change from quasi-D_{5h} to quasi-O_h. *Chem. Sci.* **2013**, *4* (8), 3310−3316.
(27) Ding, Y. S.; Chilton, N. F.; Winpenny, R. E. P.; Zheng, Y. Z. On Approaching the Limit of Molecular Magnetic Anisotropy: A Near-Perfect Pentagonal Bipyramidal Dysprosium(III) Single-Molecule Magnet. *Angew. Chem., Int. Ed.* **2016**, *55* (52), 16071−16074.
(28) Giansiracusa, M. J.; Al-Badran, S.; Kostopoulos, A. K.; Whitehead, G. F. S.; Collison, D.; Tuna, F.; Winpenny, R. E. P.; Chilton, N. F. A large barrier single-molecule magnet without magnetic memory. *Dalton Trans.* **2019**, *48* (29), 10795−10798.
(29) Wang, Y. X.; Ma, Y.; Chai, Y.; Shi, W.; Sun, Y.; Cheng, P. Observation of Magnetodielectric Effect in a Dysprosium-Based Single-Molecule Magnet. *J. Am. Chem. Soc.* **2018**, *140* (25), 7795−7798.
(30) Zeng, D.; Ren, M.; Bao, S. S.; Li, L.; Zheng, L. M. A luminescent heptanuclear DyIr6 complex showing field-induced slow magnetization relaxation. *Chem. Commun.* **2014**, *50* (61), 8356−8359.
(31) Langley, S. K.; Vignesh, K. R.; Holton, K.; Benjamin, S.; Hix, G. B.; Phonsri, W.; Moubaraki, B.; Murray, K. S.; Rajaraman, G. Mononuclear Dysprosium(III) Complexes with Triphenylphosphine Oxide Ligands: Controlling the Coordination Environment and Magnetic Anisotropy. *Inorganics* **2018**, *6* (2), 61.
(32) Xin, Y.; Wang, J.; Zychowicz, M.; Zakrzewski, J. J.; Nakabayashi, K.; Sieklucka, B.; Chorazy, S.; Ohkoshi, S. I. Dehydration-Hydration Switching of Single-Molecule Magnet Behavior and Visible Photoluminescence in a Cyanido-Bridged Dy(III)Co(III) Framework. *J. Am. Chem. Soc.* **2019**, *141* (45), 18211−18220.
(33) Gregson, M.; Chilton, N. F.; Ariciu, A.-M.; Tuna, F.; Crowe, I. F.; Lewis, W.; Blake, A. J.; Collison, D.; McInnes, E. J. L.; Winpenny, R. E. P.; Liddle, S. T. A monometallic lanthanide bis(methanediide) single molecule magnet with a large energy barrier and complex spin relaxation behaviour. *Chem. Sci.* **2016**, *7* (1), 155−165.
(34) Meng, Y. S.; Zhang, Y. Q.; Wang, Z. M.; Wang, B.-W.; Gao, S. Weak Ligand-Field Effect from Ancillary Ligands on Enhancing Single-Ion Magnet Performance. *Chem. - Eur. J.* **2016**, *22* (36), 12724−12731.
(35) Harriman, K. L.; Brosmer, J. L.; Ungur, L.; Diaconescu, P. L.; Murugesu, M. In the Pursuit of Record Breaking Energy Barriers: A Study of Magnetic Axiality in Diamide Ligated Dy^{III} Single-Molecule Magnets. *J. Am. Chem. Soc.* **2017**, *139* (4), 1420−1423.
(36) *Bruker, SMART, SAINT, and XPREP: Area Detector Control and Data Integration and Reduction Software*; Bruker Analytical X-ray Instruments Inc.: Madison, WI, 1995.
(37) Sheldrick, G. M. *SADABS, Program for Empirical Absorption Correction*; University of Göttingen: Göttingen, Germany, 1996.
(38) Dolomanov, O. V.; Bourhis, L. J.; Gildea, R. J.; Howard, J. A. K.; Puschmann, H. OLEX2: a complete structure solution, refinement and analysis program. *J. Appl. Crystallogr.* **2009**, *42* (2), 339−341.
(39) Sheldrick, G. M. A short history of SHELX. *Acta Crystallogr., Sect. A: Found. Crystallogr.* **2008**, *64*, 112−122.

https://dx.doi.org/10.1021/acs.inorgchem.0c00616
Inorg. Chem. 2020, 59, 7158−7166

(40) Spek, A. Single-crystal structure validation with the program PLATON. *J. Appl. Crystallogr.* **2003**, *36* (1), 7−13.
(41) Llunell, M. C. D.; Cirera, J.; Bofill, J. M.; Alemany, P.; Alvarez, S. *SHAPE* (version 2.1); Universitat de Barcelona, 2013.
(42) Reta, D.; Chilton, N. F. Uncertainty estimates for magnetic relaxation times and magnetic relaxation parameters. *Phys. Chem. Chem. Phys.* **2019**, *21* (42), 23567−23575.
(43) Ding, Y. S.; Yu, K. X.; Reta, D.; Ortu, F.; Winpenny, R. E. P.; Zheng, Y.-Z.; Chilton, N. F. Field- and temperature-dependent quantum tunnelling of the magnetisation in a large barrier single-molecule magnet. *Nat. Commun.* **2018**, *9* (1), 3134.
(44) Ungur, L.; Le Roy, J. J.; Korobkov, I.; Murugesu, M.; Chibotaru, L. F. Fine-tuning the Local Symmetry to Attain Record Blocking Temperature and Magnetic Remanence in a Single-Ion Magnet. *Angew. Chem., Int. Ed.* **2014**, *53* (17), 4413−4417.
(45) Aquilante, F.; Autschbach, J.; Carlson, R. K.; Chibotaru, L. F.; Delcey, M. G.; De Vico, L.; Fdez Galván, I.; Ferré, N.; Frutos, L. M.; Gagliardi, L.; et al. Molcas 8: New capabilities for multiconfigurational quantum chemical calculations across the periodic table. *J. Comput. Chem.* **2016**, *37* (5), 506−541.
(46) Chibotaru, L. F.; Ungur, L. Ab initio calculation of anisotropic magnetic properties of complexes. I. Unique definition of pseudospin Hamiltonians and their derivation. *J. Chem. Phys.* **2012**, *137* (6), 064112.
(47) Ungur, L.; Thewissen, M.; Costes, J. P.; Wernsdorfer, W.; Chibotaru, L. F. Interplay of Strongly Anisotropic Metal Ions in Magnetic Blocking of Complexes. *Inorg. Chem.* **2013**, *52* (11), 6328−6337.
(48) Shiozaki, T.; Győrffy, W.; Celani, P.; Werner, H.-J. Communication: Extended multi-state complete active space second-order perturbation theory: Energy and nuclear gradients. *J. Chem. Phys.* **2011**, *135* (8), 081106.
(49) Chen, Y.; Liu, J.; Lan, Y.; Zhong, Z.; Mansikkamäki, A.; Ungur, L.; Li, Q.-W.; Jia, J.-H.; Chibotaru, L. F.; Han, J.-B.; et al. Dynamic Magnetic and Optical Insight into a High Performance Pentagonal Bipyramidal Dy^{III} Single-Ion Magnet. *Chem. - Eur. J.* **2017**, *23* (24), 5708−5715.
(50) Li, L. L.; Su, H. D.; Liu, S.; Xu, Y. C.; Wang, W.-Z. A new air- and moisture-stable pentagonal-bipyramidal Dy^{III} single-ion magnet based on the HMPA ligand. *Dalton Trans.* **2019**, *48* (6), 2213−2219.
(51) Li, Z. H.; Zhai, Y. Q.; Chen, W.-P.; Ding, Y. S.; Zheng, Y. Z. Air-Stable Hexagonal Bipyramidal Dysprosium(III) Single-Ion Magnets with Nearly Perfect D_{6h} Local Symmetry. *Chem. - Eur. J.* **2019**, *25* (71), 16219−16224.
(52) Canaj, A. B.; Dey, S.; Martí, E. R.; Wilson, C.; Rajaraman, G.; Murrie, M. Insight into D_{6h} Symmetry: Targeting Strong Axiality in Stable Dysprosium(III) Hexagonal Bipyramidal Single-Ion Magnets. *Angew. Chem., Int. Ed.* **2019**, *58* (40), 14146−14151.

https://dx.doi.org/10.1021/acs.inorgchem.0c00616
Inorg. Chem. 2020, 59, 7158−7166